Astron. Astrophys. Suppl. **29**, 279-292.

OBSERVATIONS OF 40 LOW LUMINOSITY RADIO GALAXIES WITH THE WESTERBORK SYNTHESIS RADIO TELESCOPE

C. FANTI, R. FANTI, I.M. GIOIA, C. LARI, P. PARMA
Laboratorio di Radioastronomia CNR, Bologna, Italy
M.H. ULRICH
McDonald Observatory, University of Texas, Austin, U.S.A.
and
Observatoire de Paris, Meudon, France

Received December 17, 1976, revised March 28, 1977

The Westerbork Synthesis Radio Telescope has been used to map 40 radio galaxies at the frequencies of 610, 1415 and 4995 MHz. The results are presented here along with various physical parameters derived for the sources.

Key words: radio galaxies – radio fluxes – radio structure

1. INTRODUCTION

This is the fourth of a series of papers on the radio properties of galaxies. Previous papers (Fanti *et al.* 1973 and Colla *et al.* 1975a, hereafter called paper I and II) described the selection of a complete sample of galaxies from the "Catalogue of Galaxies and Clusters of Galaxies" (Zwicky *et al.* 1963, 1966), identified with radio sources of the second Bologna catalogue. Paper III (Colla *et al.* 1975b) gave a preliminary statistical analysis of the radio and optical properties of the galaxies of the sample and the bivariate luminosity function of the elliptical galaxies.

This paper presents new observations for 40 galaxies from the aforementioned sample, obtained at three frequencies (610, 1415 and 4995 MHz) with the Westerbork Synthesis Radio Telescope (WSRT). They allow us to obtain, for most of the galaxies, radio structures with resolutions ranging from 8 to 54 arcsec.

2. THE OBSERVATIONS AND THE DATA REDUCTION

The observations were made with the WSRT[1] at 610, 1415 and 4995 MHz. For each source and frequency three to ten short observations (each not less than ten minutes in length) were made at widely spaced hour angles (see table 1), giving a sampling of the $U-V$ plane ranging from at least sixty to two hundred points. These data, calibrated with the standard procedure by the reduction group in Leiden, were used to perform a Fourier Transform, producing a bidimensional map. This map, the so-called "dirty map", due to the incomplete coverage of the $U-V$ plane, is severely affected by strong sidelobes which make the interpretation of the source structure very difficult.

We used, therefore, the so-called "clean" technique to remove the effect of the undesired sidelobes responses. The "clean" technique is described by Högbom (1974) and the reader is referred to it for details. Here we only remember that the reliability of the cleaned maps rests on the assumption that the synthesized map is mostly empty, or, in other words, that the sky brightness is zero almost everywhere. Therefore, maps of radio sources of large scale structure, or of fields in which there are many radio sources, have to be considered with caution. Moreover, this procedure does not eliminate confusion problems originated by sidelobes of radio sources outside the synthesized field. To reduce this problem we have computed maps

[1] The WSRT, its mode of operation, its performance and data processing are described by Baars *et al.* (1974), Casse *et al.* (1974), and Högbom *et al.* (1974).

40 × 40 arcmin in size at 1415 MHz and 80 × 80 arcmin at 610 MHz. These sizes are slightly larger than the half-power beam width of the individual dishes, and therefore contain most of the confusing sources in the field of view of the telescope.

At 4995 MHz the expected number of sources per primary beam is very small, so that, in general, only small fields (3 × 3 arcmin) have been synthesized.

Table 1 gives the number of short observations used at each frequency for each source and the rms of the response in each map, computed on the map itself. This figure, at 4995 MHz, is fully due to the noise. At 1415 MHz and especially at 610 MHz, it is mostly due to confusion from sidelobes of sources outside the synthesized map.

Radio sources from the original sample (see paper II) missing here were not observed either because better quality radio maps were already available (see references quoted in paper II) or because, being of very small size, further information was not useful (see paper II). For the two radio galaxies 3C 338 (B2 1626+39) and 3C 382 (B2 1833+32) better maps became available from other authors (Jaffe and Perola 1974, Riley *et al.* 1973) after this work was started. Our maps are displayed in figure 2 with those of the other sources. They may help in judging the reliability of maps of complex sources, when observed with our procedure. Full synthesis maps at 1415 MHz for 0326+39, 1321+31, 1422+26, 1615+35 and 1621+38 will be published elsewhere. A full synthesis map of 0924+30 at 1415 MHz has been published by Ekers *et al.* (1975).

The radio source 0910+35 was undetected at 6 cm and severely confused at 21 and 50 cm by nearby very strong radio sources.

3. THE DATA

Table 2 lists the results of the observations. They are arranged as follows:

Column 1: B2 name.

Column 2: Radio component name (G means optical galaxy, c: core, E: extended component, T: total flux, a, b, A, B, C, D: other components).

Columns 3, 4: Right ascension and declination of centroids of the radio components.

Columns 5, 6, 7, 8: The 408, 610, 1415 and 4995 MHz flux densities in mJy; single bracket signs indicate cases where the flux densities are the total flux densities from two or more components. For the 408 MHz flux density scale, the reader is referred to the B2 catalogue of radio sources. The 610, 1415 and 4995 MHz flux density scale is that of Kellermann *et al.* (1969).

Column 9: Redshift (taken from paper II).

Column 10: Half-power width of the source parallel and perpendicular to the major axis (gaussian model), position angle of the major axis.

Column 11: Absolute magnitude of the galaxy.

Column 12: Logarithm of radio luminosity at 1415 MHz.

Column 13: Overall linear dimensions in kpc.

Column 14: Estimate of the minimum energy in the source. The formula used is that given by McDonald *et al.* (1968), decreased by a factor 13.9, as it is assumed that there are no relativistic protons in the source.

Column 15: The equipartition magnetic field.

Column 16: The minimum energy density in the source.

We have used a Hubble constant $H=100$ km s^{-1} Mpc^{-1} instead of $H=50$ km s^{-1} Mpc^{-1} to make a comparison with our previous papers (I, II and III) easier. At any rate, we give the conversion formulae to $H=50$ for the following quantities: $M_{50}=M_{100}-1.5$, $\log P_{50}=\log P_{100}+0.6$, $D_{50}=D_{100}\times 2$, $U_{\min 50}=U_{\min 100}\times 5.38$, $H_{\min 50}=H_{\min 100}/1.22$, $u_{\min 50}=u_{\min 100}/1.49$.

Figure 1 shows a comparison of the 1415 MHz fluxes measured here and those reported in paper II, obtained with the Nançay radio telescope.

Radio maps of 32 radio galaxies are shown in figure 2. For each source we give in general only maps showing structure. The maps of 8 sources which are unresolved or just slightly resolved are not shown. The position of the galaxy is marked in each map by a cross. Contour levels are, in general, integer multiples of a given value (different from map to map) indicated in the figures. Zero and negative levels are omitted for clarity. The beam size in each map is represented by an L shape, whose arms are the half-power width in EW and NS. In general, the beam widths are $(7.6'' \times 7.6''/\sin\delta)$ at 4995 MHz, $(24'' \times 24''/\sin\delta)$ at 1415 MHz and $(54'' \times 54''/\sin\delta)$ at 610 MHz. In a few cases (see comments on individual galaxies) maps are convolved with gaussian function to decrease the resolution in order to display low brightness features. Finding charts of the galaxies, taken from the red prints of the Palomar Sky Survey, are given in paper II.

4. COMMENTS ON INDIVIDUAL GALAXIES

0034+25 The source is an asymmetric double, with one component on the optical galaxy and a second one $\sim 2.5'$ towards the east. A core source is detected at 4995 MHz (~ 10 mJy). The map at 610 MHz suggests the existence of a third component of ~ 30 mJy (6σ), SW of the galaxy.

0055+30 The 1415 MHz map of this source has already been published (Fanti *et al.* 1976). The source is dominated by a very strong nuclear source of small diameter ($< 0.1''$) and flat or rising spectrum (see previous reference). The NW component has an asymmetrical shape, typical of a "head-tail" source. Its 610-1415 MHz spectral index steepens, from about 0.5 to > 1.0, going from the inner to the outer parts. The SE component is undetected at 6 cm and has a steep spectrum ($\alpha \simeq 1.4$). The galaxy may belong to the Zwicky cluster ($01^h07^m.5+32°12'$). Recently Bridle *et al.* (1976) have shown that our source is the central part of a giant radio source 0.7 Mpc in size.

0055+26 The source is too extended to be mapped with the full resolution at 4995 MHz. The comparison of the 1415 MHz map and of the 4995 MHz one, convolved to the resolution of the former, indicates that the spectrum of the two outermost components is rather steep ($\alpha > 1.0$ for the most western: $\alpha \sim 1.2$ for the NE), while the main components have a normal spectrum ($\alpha \sim 0.6$).

0120+33 The radio source, detected at 1415 MHz, is displaced west of the center of the galaxy by $\sim 15''$, but it is still well within the main body of it. At 610 MHz a second component may have been detected, at a level of 40 mJy ($\sim 6\sigma$) east of the galaxy. The WSRT 1415 MHz flux density is significantly lower than the total power flux density from the Nançay telescope (reported in paper II), suggesting a low brightness large scale structure. The galaxy belongs to the Zwicky cluster ($01^h07^m.5+32°12'$).

0149+35 See Wilson *et al.* (1977) for a 610 MHz map of this source. The central source coincides with the galaxy NGC 708, the brightest of the Abell cluster A262. The southern source is associated to the spiral galaxy NGC 710. The northern source is not associated to any optical object and may not be connected to NGC 703. At 4995 MHz only the northern source is detected. The southern one was out of the observed field. A new source is detected at 4995 MHz and coincides with the nucleus of the galaxy NGC 703. Its flux is 9 mJy and the radio spectrum is flat.

0206+35 The source was observed at only 3 p.a., and since its structure is rather complex, the full resolution cleaned map is not reliable. The source is dominated by a bright core with flat spectrum. The extended source is elongated in p.a. 124°, possibly double.

0326+39 The source is triple (see 610 MHz map), with the central component again triple (see 4995 MHz map). The central component is unresolved. This source has been observed in a full synthesis at 1415 MHz at Westerbork (Ekers *et al.*, in preparation).

0755+37 The source is too extended to be mapped at full resolution at 4995 MHz. The map given in figure 2 at this frequency has a resolution of 16×16 arcsec. The core has a flat spectrum. The extended outer components have a spectral index $\alpha \sim 0.7$.

0800+24 The radio source is very complex and asymmetrical. A core source with spectral index $\alpha < 0.2$ coincides with the nucleus of the galaxy. Another point source, 3.5′ SW may be unrelated to the galaxy. Its spectrum is rather flat.

0844+31 See Grueff and Vigotti (1974) for a 6 cm map. A 1415 MHz map has been obtained at Westerbork by Miley (private communication).

0915+32 The source is too extended and low in brightness to be mapped at full resolution at 4995 MHz. Two galaxies (E and SO?) are located between the central and northern component. Due to the lack of any compact component in either galaxy, we do not know which galaxy is responsible for the radio emission.

0916+34 The two components are asymmetrically located with respect to the galaxy just outside its main body. It could be a misidentification. Note, however, the possible similarity with 0800+24 (1415 MHz map), if one doesn't consider the core source. The galaxy is near the edge of the Abell cluster A779.

1040+31 Triple system of galaxies in a common halo. The core of the radio source is nearer to the central galaxy (the brighter), whose position is marked on the radio map.

1108+27 The source seems associated to the eastern end of a pair of galaxies, which coincide (within the errors) with an unresolved radio component. The radio source is asymmetric with respect to the galaxy and looks like a "head-tail" source.

1113+29 A higher resolution map has been published by Riley (1975). The radio source is associated to the northern galaxy of a double system belonging to the Abell Cluster A1213. A second radio source, with flat spectrum, detected also by Riley (1975) is associated to another elliptical galaxy, probably the brightest of the cluster. Its fluxes are 40 mJy at 1415 MHz and 60 mJy at 4995 MHz.

1317+33 Two elliptical galaxies in common halo. The radio source coincides with the western galaxy.

1318+34 Zwicky compact galaxy, reported also in the Arp Atlas of Peculiar Galaxies (Arp 1966). See also Sargent (1970) for a description of it.

1422+26 This source has been observed in a full synthesis at Westerbork at 1415 MHz (Ekers *et al.*, in preparation).

1525+29 The radio source is associated to the second brighter galaxy of the Abell Cluster A2079.

1553+24 The radio source is dominated by a strong core and has possible very weak outer components.

1602+34 Triple source of very low brightness. It is undetected both at 6 and 21 cm. The galaxy is shifted $\sim 1'$ from the radio axis and very likely may be a misidentification.

1855+37 A point source coincides with the nucleus of the galaxy. A second component is about 2′ west of it and may not be associated to the galaxy.

2229+39 The 4995 MHz map presented here has a resolution of 24×39 arcsec.

ACKNOWLEDGMENTS

We are grateful to the observational staff at Westerbork and to the reduction staff at Leiden. We also wish to thank Mr. L. Baldeschi and Mr. R. Primavera for their collaboration in preparing the drawings and graphics.

The Westerbork Synthesis Radio Telescope is operated by the Netherlands Foundation for Radio Astronomy with the financial support of the Netherlands Organization for the Advancement of Pure Research (Z.W.O.).

REFERENCES

Arp, H.C.: 1966, *Astrophys. J. Suppl.* **14**.
Baars, J.W.M. and Hooghoudt, B.G.: 1974, *Astron. Astrophys.* **31**, 323.
Bridle, A.H., Davis, M.M., Meloy, D.A., Fomalont, E.B., Strom, R.G. and Willis, A.G.: 1976, *Nature* **262**, 179.
Casse, J.L. and Mueller, C.A.: 1974, *Astron. Astrophys.* **31**, 333.
Colla, G., Fanti, C., Fanti, R., Gioia, I., Lari, C., Lequeux, J., Lucas, R. and Ulrich, M.H.: 1975a, *Astron. Astrophys. Suppl.* **20**, 1.
Colla, G., Fanti, C., Fanti, R., Gioia, I., Lari, C., Lequeux, J., Lucas, R. and Ulrich, M.H.: 1975b, *Astron. Astrophys.* **38**, 209.
Ekers, R.D., Fanti, R., Lari, C. and Ulrich, M.H.: 1975, *Nature* **258**, 584.
Fanti, R., Gioia, I., Lari, C., Lequeux, J. and Lucas, R.: 1973, *Astron. Astrophys.* **24**, 69.
Fanti, R., Lari, C., Spencer, R.E. and Warwick, R.S.: 1976, *Monthly Notices Roy. Astron. Soc.* **174**, 1P.
Grueff, G. and Vigotti, M.: 1973, *Astron. Astrophys. Suppl.* **11**, 41.
Högbom, J.A. and Brouw, W.N.: 1974, *Astron. Astrophys.* **33**, 289.
Högbom, J.A.: 1974, *Astron. Astrophys. Suppl.* **15**, 417.
Jaffe, W. and Perola, G.C.: 1974, *Astron. Astrophys.* **31**, 223.
Kellermann, K.I., Pauliny-Toth, I.K. and Williams, P.J.S.: 1969, *Astrophys. J.* **157**, 1.
McDonald, G.H., Kenderdine, S. and Neville, A.C.: 1968, *Monthly Notices Roy. Astron. Soc.* **138**, 259.
Riley, J.H. and Branson, N.J.B.A.: 1973, *Monthly Notices Roy. Astron. Soc.* **164**, 271.
Riley, J.H.: 1975, *Monthly Notices Roy. Astron. Soc.* **170**, 53.
Sargent, W.L.W.: 1970, *Astrophys. J.* **159**, 765.
Wilson, A., Vallée, J., Lari, C. and Parma, P.: 1977, in prep.

C. Fanti
R. Fanti
I.M. Gioia
C. Lari
P. Parma

Laboratorio di Radioastronomia
c/o Istituto di Fisica
Via Irnerio 46
I–40126 Bologna (Italy)

M.H. Ulrich

European Southern Observatory
c/o CERN
T.P. Division
CH–1211 Geneva 23

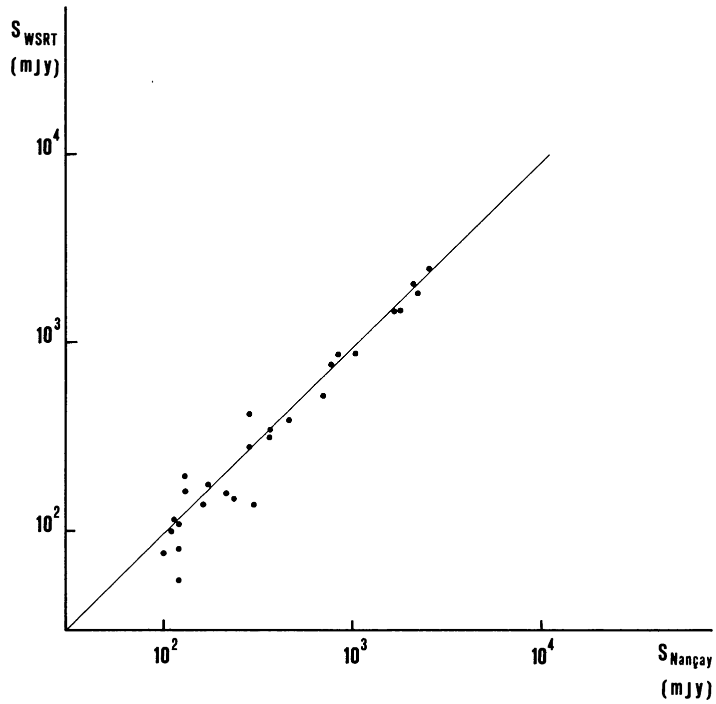

Figure 1 Comparison between 1415 MHz fluxes measured at Nançay and at Westerbork.

Table 1 Observational Parameters

Name	610 MHz		1415 MHz		4995 MHz	
	number of observations	r.m.s. mJy/beam	number of observations	r.m.s. mJy/beam	number of observations	r.m.s. mJy/beam
0034+25	9	4.8	8	2.5	6	1.5
0055+30	6	6.0	7	3.0	5	5.7
0055+26	7	5.7	7	3.1	6	3.5
0120+33	10	7.1	10	3.3	--	---
0149+35	--	---	8	2.3	6	1.5
0206+35	5	4.4	6	5.0	3	8.0
0222+36	6	3.8	6	3.5	3	4.0
0326+39	7	5.9	--	---	6	2.0
0331+39	5	4.5	--	---	5	2.5
0648+27	6	4.1	5	3.3	5	2.1
0722+30	6	4.0	5	3.4	6	1.9
0755+37	7	5.0	7	6.3	7	5.0
0800+24	--	---	7	2.5	6	1.5
0836+29	6	5.7	6	2.8	6	3.0
0844+31	7	4.1	--	---	--	---
0915+32	10	5.7	8	2.5	7	4.0
0916+34	7	4.5	--	---	6	2.9
1040+31	5	4.5	6	3.6	7	3.2
1102+30	7	3.9	7	2.8	6	3.2
1108+27	7	3.4	7	2.2	6	3.0
1113+29	5	4.1	6	3.5	6	4.3
1122+39	7	3.3	--	---	3	2.4
1254+27	--	---	--	---	6	1.5
1317+33	--	---	6	2.7	7	1.8
1318+34	6	3.7	--	---	6	2.5
1322+36	5	4.6	6	3.5	6	2.1
1346+26	7	4.0	6	4.9	6	2.5
1350+31	--	---	--	---	6	6.5
1422+26	8	5.5	--	---	6	2.7
1506+34	--	---	6	3.5	6	1.5
1525+29	8	3.8	7	3.7	6	2.5
1553+24	9	4.5	9	2.2	6	2.8
1602+34	8	3.7	--	---	--	---
1610+29	7	3.5	5	3.1	--	---
1626+39	--	---	--	---	6	3.9
1833+32	4	5.6	--	---	4	8.0
1855+37	8	3.5	9	3.1	6	1.7
2116+26	7	4.0	4	3.2	6	1.5
2229+39	4	7.0	--	---	6	4.5
2236+35	6	3.8	6	3.0	5	2.2

Table 2

NAME		R.A. h m s	DEC. ° ′ ″	FLUX (mJy) 408	610	1415	5000	Z	$\theta_1 \times \theta_2$ (P.A.) arcsec (deg)	M_{pg}	LOG P 1415	D(Kpc)	U_{min} 10^{54} erg	H_{min} 10^{-6} gauss	u_{min} 10^{-12} erg/cm^3
0034+25	G	003426.8	252526					.0321		-20.2	22.95				
	A	26.8	30	270	130	30	22		13X10 (90)			6X5	3.4	4.4	1.5
	B	32.0	16			50	-		40X15 (108)			19X7	10.4	2.9	.6
0055+30	G	005505.6	300456					.0167		-21.2	23.65				
	c	05.7	57	360	400	400	670		<0.1			<.02			
	A	02.7	0525	2400	1664	1000	500		130X20 (130)			33X5	25.2	5.0	1.9
	B	16.0	0300		260	70	~10		60X40 (90)			15X10	7.1	1.9	.3
0055+26	G	005540.7	263544					.0472		-21.0	24.61				
	A	39.4	3600	4900	3150	800	385		23X39 (20)			16X28	185	4.6	1.7
	B	45.0	3600			810	300		30X70 (40)			21X50	202	3.4	.8
	C	34.0	3520			90	5								
0120+33	G	012050.7	325945					.0164		-20.7	22.20				
	A	49.5	50	690	180	~55			~50 (90)			12.3	2.5	1.7	.2
0149+35	G	014950.0	355420					.0160		-19.1	22.69				
	A	44.3	5658	360		30	10								
	B	49.6	5417			90	<5		54 (80)			13	3.8	2.1	.3
	C	58.4	4840			57	-		50 (50)			12	2.3	1.7	.2
0206+35	G	020639.3	353341					.0375		-20.7	24.50				
	c	39.2	42	4560	3356	2100	240								
	T	39.2	40				970		45X20 (120)			25X11	176	6.6	3.5
0222+36	G	022223.9	365657					.0327		-20.3	23.62				
	c		56	340	297	280	185		<2			<.98			
0326+39	G	032606.5	393712					.0243		-20.0	23.68				
	a	05.0	12	1900	400		35		13X 6 (12)			5X2	1.8	8.1	5.3
	c	06.4	14				70		<5			<1.8			
	b	08.0	17				12		7 (123)			2.6	.9	6.4	3.3
	A	2556.0	38		560		350		100X70 (20)			36X25	84	1.6	.2
	B	2616.0	10		600				110X80 (0)			40X29	101	1.8	.2
0331+39	G	033101.0	391125					.0202		-20.5	23.61				
	c	00.9	23	1720	1280		250								
	E						250		24X 8 (180)			7X2	6.5	10.6	9.9
0648+27	G	064854.9	273118					.0409		-21.3	23.43				
	c	54.8	18	270	210	150	60		<5			<3.1			
0722+30	G	072227.5	300314					.0191		-18.6	22.64				
	c	27.4	17	380	195	110	80		12X 8 (180)			3X2	1.6	8.3	5.8
0755+37	G	075509.2	375522					.0413		-20.7	24.67				
	c	09.1	22	5900	4150	≤325	250								
	A	05.7	33			≥2200	450		35X35			22X22	219	4.2	1.4
	B	13.1	11				450		35X35			22X22	219	4.2	1.4
0800+24	G	080016.3	244902					.0433		-20.1	23.52				
	c	16.2	01	320		124	12		90X40 (36)			58X20	120	1.5	.2
	A	14.6	04				65								
	B	07.0	4620			40	18								
0836+29	G	083659.1	295945					.0650		-20.9	24.38				
	A	58.3	27	1560	990	530	103		11X 6 (30)			11X6	37	9.0	6.5
	B	59.2	50				150		22X11 (36)			21X11	106	5.8	2.7
0844+31	G	084454.2	315812					.0675		-21.1	24.82				
	A	57.1	5645	3750	1260				70X40 (95)			71X40	808	2.3	.4
	B	53.0	5945		1360				75X60 (100)			76X61	1240	1.8	.3
0915+32	G	091557.0	320351					.0620		-20.9	24.24				
	G	58.5	0421												
	A	51.0	0145	470	105	85	40		60X53 (20)			56X49	247	1.1	.11
	B	56.3	37		303	205	79		80X60 (56)			74X56	513	1.2	.14
	C	1600.0	0530			130	72		70X60 (0)			65X56	372	1.1	.11
0916+34	G	091614.3	341311					.0232		-18.6	22.99				
	A	11.8	40	640	450		47		13X 9 (90)			4X3	2.9	7.5	4.3
	B	13.9	32				57		12X 7 (171)			4X2	2.6	9.3	6.7
1040+31	G	104031.0	314645					.0360		-19.6	24.03				
	c	31.2	49	1690	1010	767	50								
	E						380		30X20 (55)			16X11	74.4	5.7	2.5
1102+30	G	110239.7	302553					.0720		-20.9	24.34				
	c	39.7	53			<20	24								
	A	36.1	30	960	225	150	60		50 (70)			54	429	1.4	.17
	B	43.0	2605		420	245	69		50 (60)			54	573	1.7	.2
1108+27	G	110843.4	271406					.0331		-20.3	23.07				
	c	44.0	07	200	110	100	22								
	A	43.1	06				≥20		40			19.9	26.1	1.9	.3
	B	42.4	03				≥10								
1113+29	G	111353.4	293134					.0489		-20.7	24.68				
	c	53.5	36			1200	60								
	A	52.0	35	4950	3280		500		20 (80)			14.7	170	5.7	3.1
	B	56.0	3200			640	300		27X30 (90)			20X22	181	4.1	1.3
1122+39	G	112201.4	390219					.0067		-19.9	21.73				
	A	00.9	18	290	120		60		14X10 (90)			1X1	.1	8.3	5.9
	B	02.7	07				30		8X 4 (120)			1X0.4	.03	13.4	15.2
1254+27	G	125459.4	274602					.0249		-20.6	22.73				
	A	59.0	4555	210			9		10			4	1.7	5.1	2.2
	B	59.3	4616				12		13 (70)			5	2.9	4.4	1.7
1317+33	G	131755.8	332419					.0379		-20.3	23.08				
	A	55.7	17	240		77	34		10 (40)			6	7.9	5.9	2.7
1318+34	G	131816.9	342356					.0232		-19.3	22.91				
	A	17.0	2404	220	170		55		11 (150)			4	3.7	7.3	4.3
1322+36	G	132235.4	363819					.0175		-19.6	23.67				
	c	35.3	19	1710	1240	860	180		<4 (90)			<1			
	A	35.3	04				172		10 (90)			3	2.5	10.8	9.2
	B	35.4	36				150		10 (90)			3	2.4	10.4	8.5
1346+26	G	134634.1	265028					.0633		-20.9	24.59				
	A	33.8	25	3150	1920	890	245		6 (115)			6	57.5	16.4	19.8
1350+31	G	135003.5	314130					.0452		-20.0	25.02				
	c	03.3	32	10150			1500								
	A	4958.0	4226				140		20 (20)			14	74.8	5.1	1.9
1422+26	G	142226.5	265102					.0370		-19.6	24.36				
	c	26.5	00	2020	1270		20								
	A	23.7	00				190		44X 8 (86)			24X4	45.1	8.9	6.1
	B	28.8	02				145		32X20 (95)			18X11	74.4	9.3	2.2
1506+34	G	150605.6	343418					.0452		-20.0	23.82				
	A	05.4	49	260		195	49								
1525+29	G	152539.6	290528					.0653		-21.1	23.87				
	A	39.8	26	430	316	160	99		20X10 (30)			19X10	60.2	5.1	2.0
1553+24	G	155356.3	243532					.0426		-20.1	23.44				
	c	56.1	34	200	200	140	69								
	E						~50								
1602+34	G	160252.2	344512					.0316		-19.6	22.99				
	A	0300.0	4618	250	100				50X10 (80)			24X5	4.6	2.6	.5
	B	0250.1	4618		290				40X10 (110)			19X5	7.4	3.7	1.1
	C	0244.7	4625		65				40X 5 (10)			19X2	1.8	3.6	1.0
1610+29	G	161036.6	293652					.0313		-20.1	23.08				
	A	32.6	23	320	185	50			60X40 (51)			28X19	27.2	1.4	.17
	B	37.3	44			63			60X40 (60)			28X19	31.1	1.5	.19
1626+39	G	162655.6	393936					.0303		-21.1	24.41				
	c	55.3	37	18120			136								
	A	53.0	30				160		30X20 (152)			14X9	62.1	7.1	3.5
	B	57.0	30				200		30X20 (35)			14X9	70.8	7.6	4.0
1833+32	G	183312.0	323918					.0586		-21.0	25.32				
	c	12.0	18	13700			160								
	A	16.0	50		6300		1700		70X30 (90)			61X26	1020	4.4	1.5
	B	09.0	3816		3600		1700		80X40 (90)			70X35	1390	3.6	1.0
1855+37	G	185554.3	375627					.0552		-21.8	24.02				
	c	54.2	28	800	487	260	100								
	A	5605.6	5548		95	55	-								
2116+26	G	211620.7	261408					.0164		-20.0	22.61				
	c	20.8	10	320	160	141	60								
	E						45		50X12 (22)			12X3	3.3	5.2	2.0
2229+39	G	222907.6	390604					.0181		-19.7	24.04				
	A	06.4	0423	6450	2930		370		36X26 (2)			10X7	22.6	6.2	2.9
	B	08.0	0600				317		74X32 (11)			20X9	33.4	4.2	1.4
	C	06.6	0734				264		28X26 (90)			8X7	17.3	6.0	2.9
	D	06.5	0830				100		33 (90)			9	13.1	3.8	1.1
2236+35	G	223612.3	350411					.0277		-19.9	23.45				
	A	11.5	02	770	440	343	103		13X 7 (60)			5X3	4.9	9.3	6.9
	B	13.1	16				87		14X 7 (10)			6X3	1.2	4.5	1.6

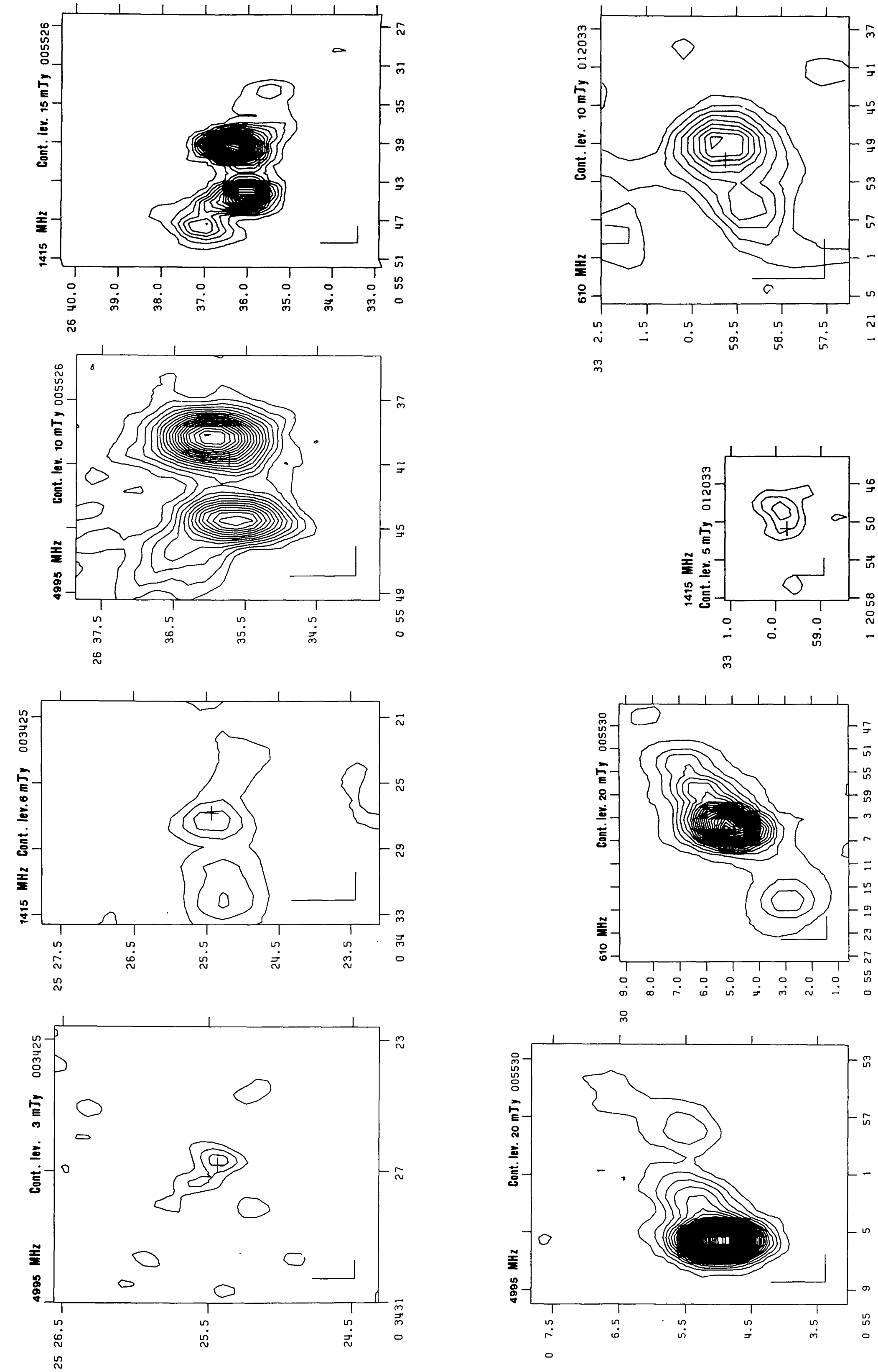

Figure 2 Contour maps. The values in mJy of the first contour level and that of the constant increment between two adjacent contours are given at the top of each map. The L-shaped sign in the lower corner is the half-power beam width. The cross represents the optical position.

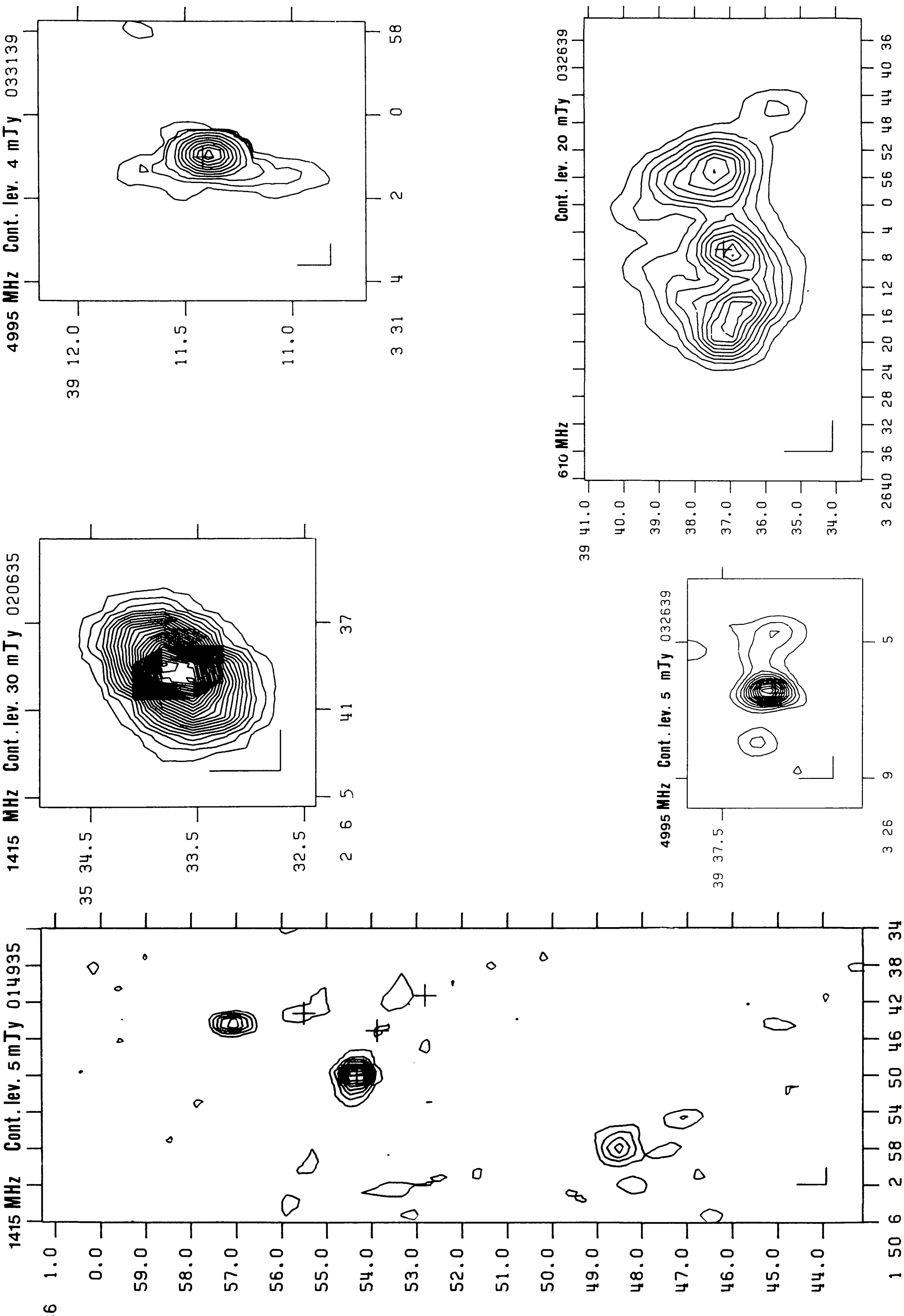

Figure 2 *(continued)*

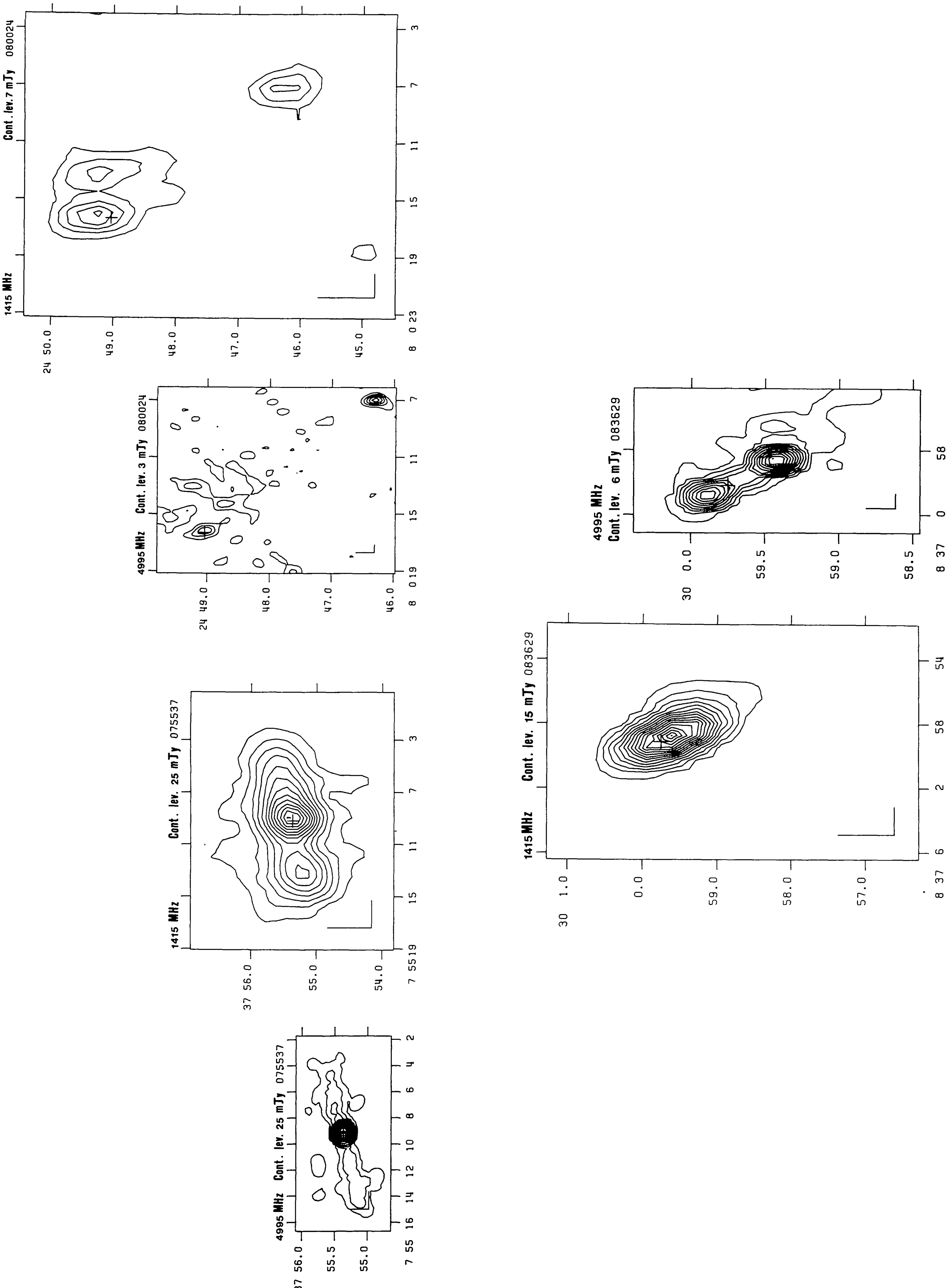

Figure 2 *(continued)*

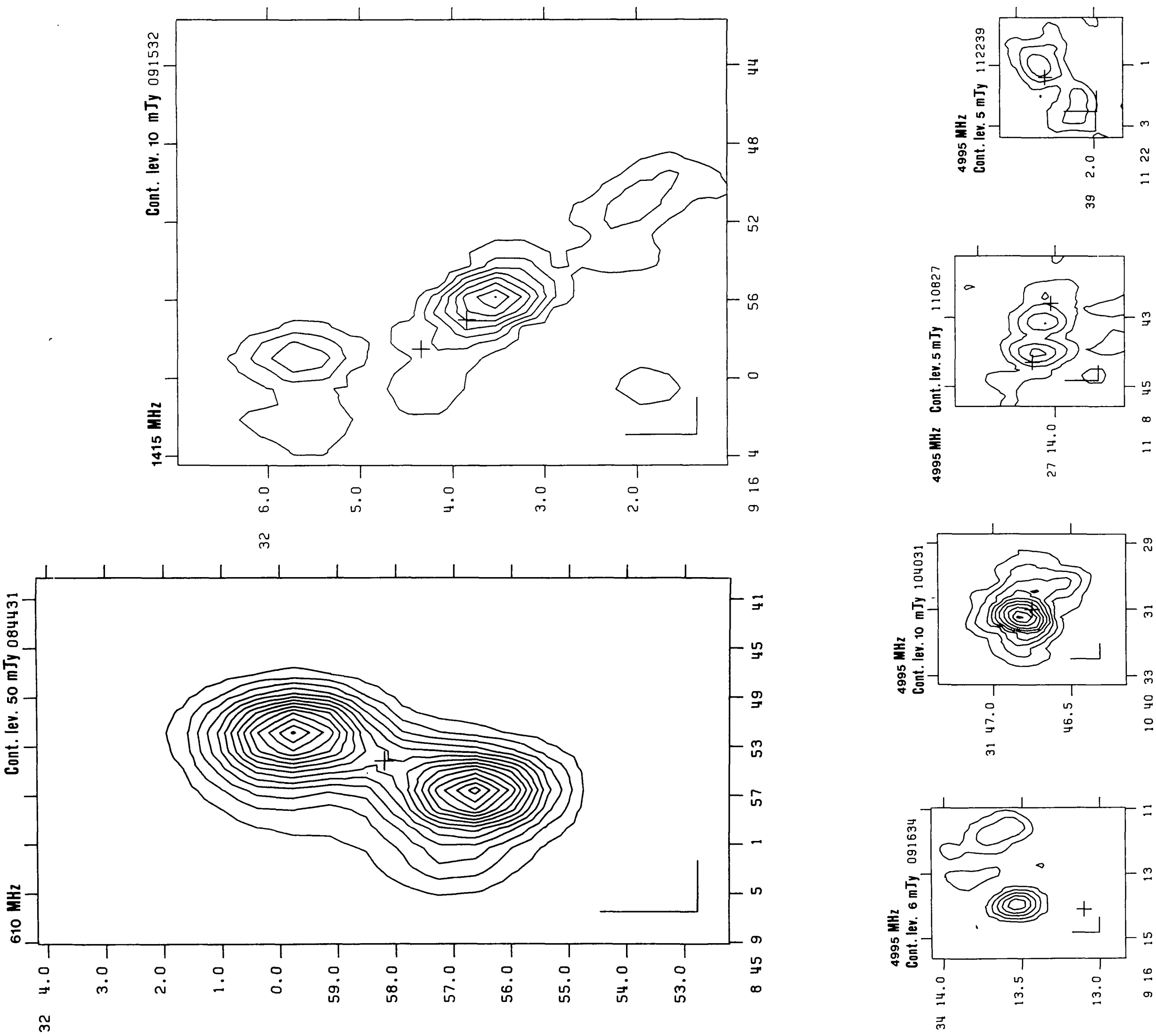

Figure 2 *(continued)*

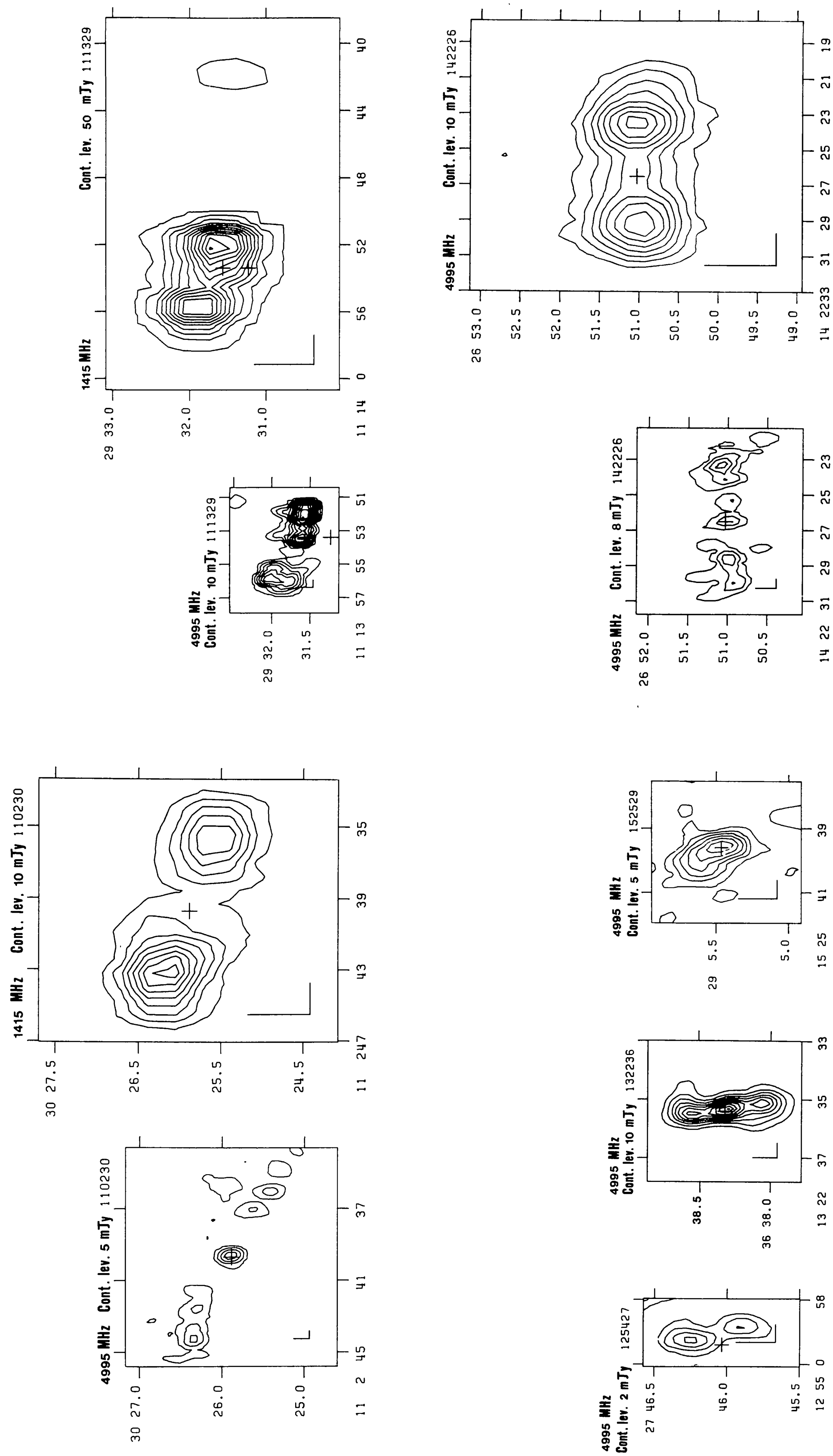

Figure 2 *(continued)*

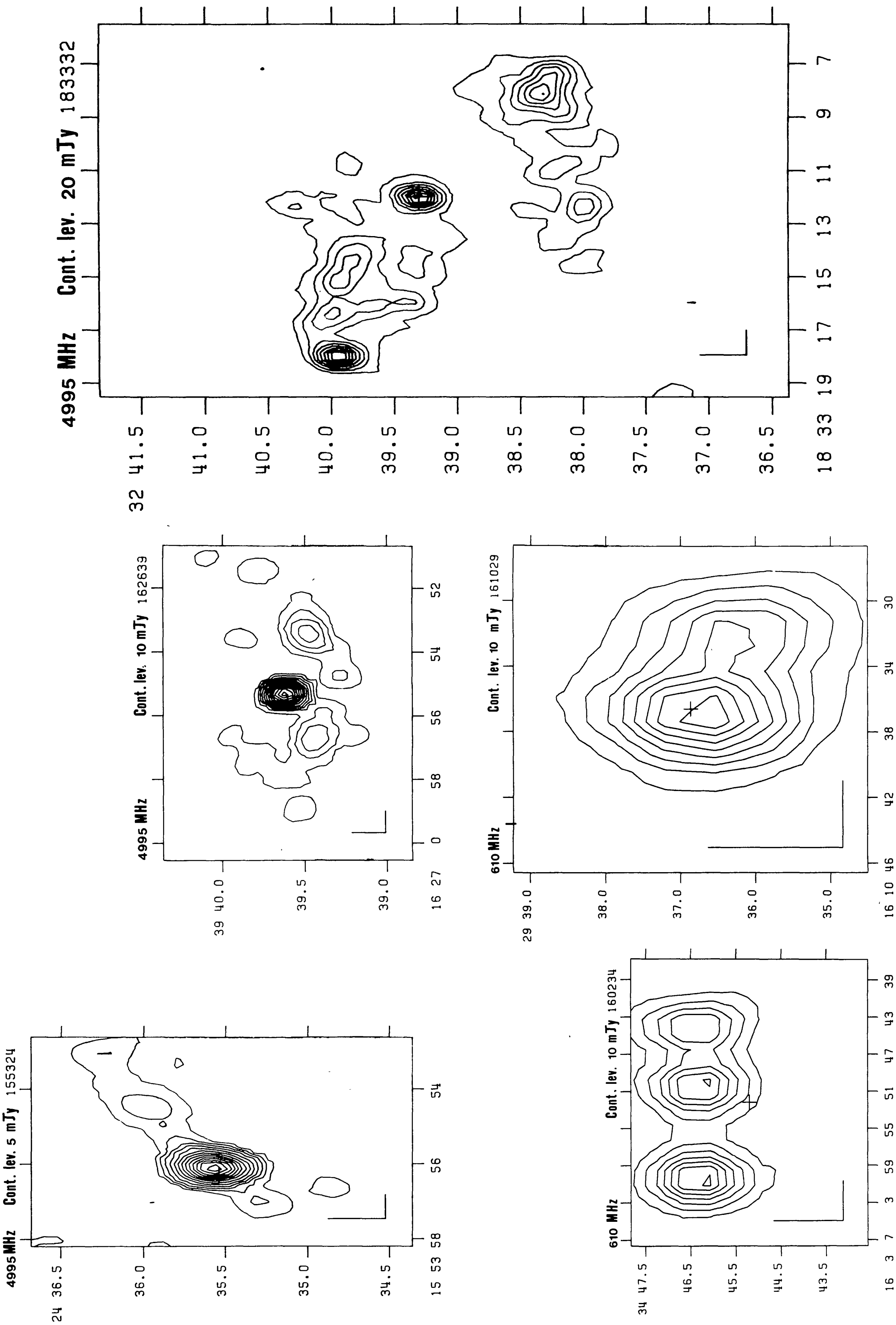

Figure 2 *(continued)*

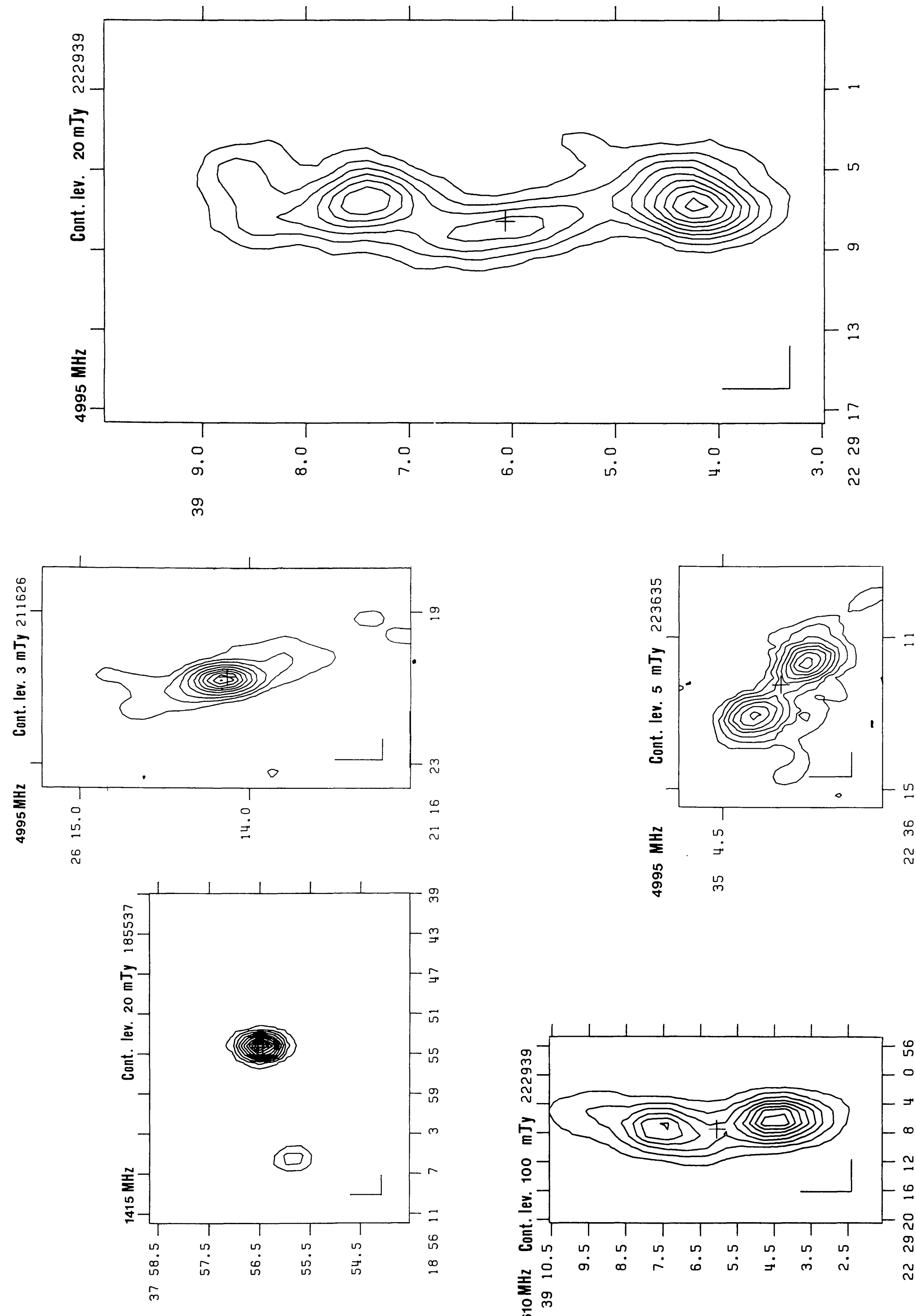

Figure 2 (continued)